Nuclear Magnetic Resonance Spectroscopic Investigations of Phase Biaxiality in the Nematic Glass of a Shape-persistent V-shaped Mesogen

ARTICLE *in* THE JOURNAL OF CHEMICAL PHYSICS · NOVEMBER 2010

Impact Factor: 2.95 · DOI: 10.1063/1.3496491 · Source: PubMed

Nuclear magnetic resonance spectroscopic investigations of phase biaxiality in the nematic glass of a shape-persistent V-shaped mesogen

João L. Figueirinhas,[1,2,a)] Gabriel Feio,[3] Carlos Cruz,[1,2] Matthias Lehmann,[4] Christiane Köhn,[4] and Ronald Y. Dong[5]
[1]*Departamento de Física, IST-TU-Lisbon, Av. Rovisco Pais, P-1049-001 Lisboa, Portugal*
[2]*CFMC, Av. Prof. Gama Pinto, 2, P-1649-003 Lisboa, Portugal*
[3]*CENIMAT/I3N, Departamento de Ciência dos Materiais, Faculdade de Ciências e Tecnologia, FCT, Universidade Nova de Lisboa, 2829-516 Caparica, Portugal*
[4]*Institute of Chemistry, Chemnitz University of Technology, Straße der Nationen 62, 09111 Chemnitz, Germany*
[5]*Department of Physics and Astronomy, University of British Columbia, Vancouver, B.C. V6T 1Z1, Canada*

(Received 4 May 2010; accepted 14 September 2010; published online 3 November 2010)

Deuterium and carbon-13 NMR spectroscopy were used to study both the high temperature uniaxial nematic and the low temperature biaxial nematic glass of a shape-persistent V-shaped mesogen. It was found that biaxial ordering determined in the domains of the latter has symmetry lower than D_{2h} and is compatible with C_{2h} symmetry or lower. In particular, elements of the ordering matrix including biaxial phase order parameters were determined from ^2H NMR at two temperatures, one just below the glass transition, and the other deep inside the biaxial glass, which allowed for the characterization of the dominant molecular motions at these temperatures. ^{13}C NMR magic angle spinning sideband patterns, collected both in the high temperature nematic phase and in the nematic glass, clearly show the difference between them in terms of the phase symmetry. © *2010 American Institute of Physics*. [doi:10.1063/1.3496491]

I. INTRODUCTION

The biaxial nematic phase (N_B) in liquid crystals (LC), theoretically predicted by Freiser in 1970,[1] exhibits in addition to the long range orientational order along the principal director $\boldsymbol{n}$, a characteristic typical of uniaxial nematics (N_U), also long range orientational order along a secondary director $\boldsymbol{l}$ that is orthogonal to $\boldsymbol{n}$. This prediction was followed a decade later by the discovery of such a mesophase in a narrow region of the phase diagram of a lyotropic LC.[2] During quite a long period, much efforts have been spent to find this elusive N_B phase in low molecular mass LC using different molecular structures and synthetic approaches.[3] In particular, in last years, a number of V-shaped molecules have been reported to be most promising in giving the N_B phase.[4–7] Up to very recently, only the simplest N_B phase with D_{2h} symmetry has been considered either theoretically or in experimental data interpretation. However, recent studies have shown other possibilities including the N_B with C_{2h} symmetry.[8] Biaxial nematic ordering has also been reported in thermotropic liquid crystals of specific mesomorphic systems with particular properties.[9,10]

At the present moment, thermotropic LC systems in which biaxial nematic order has been observed may be generally classified into three categories:

(a) bent core or V-shaped LC compounds (BLC) (Refs. 4–7)
(b) side-on polymers[9]
(c) side-on low generation dendrimers.[10]

In the first case (a), two configurations (i) and (ii) have been observed that are schematically shown in Fig. 1.[4,6] The main director $\boldsymbol{n}$ is defined in (i) by the average orientation of a long molecular axis lying in the molecular plane and normal to the molecular bisector and in (ii) by the average orientation of the normal to the molecular plane. The secondary director ($\boldsymbol{l}$) which defines the presence of the biaxial N_B phase is established by the breaking of the rotational symmetry of the V-shaped molecules about their long axis in (i) or the normal to the molecular plane in (ii) (see Fig. 1). The uniaxial-biaxial phase transition arises from the onset of a certain degree of collective rotational anisotropy of the bent direction in the plane perpendicular to the rotation axis referred above.

In cases (b) and (c), the appearance of the biaxial nematic ordering has been explained by the hindering of rotational reorientations of the mesogenic units around their most ordered axes due to the linkage with the polymeric chain (b) (Ref. 9) or with the dendritic core (c).[10]

The biaxial nematic phase has also been theoretically predicted for mixtures of disklike with rodlike mesogens.[11–16] This approach raises the problem of miscibility between chemically dissimilar units. Nevertheless, recent considerable advances have been achieved on this topic, both on simulations[17] and on the synthesis of systems of promising properties for this purpose.[18] In this work, we have studied a shape-persistent V-shaped mesogen whose molecular structure can clearly be identified as type (a). The existence of four lateral flexible alkyl chains is expected to induce

a)Author to whom correspondence should be addressed. Electronic mail: figuei@cii.fc.ul.pt.

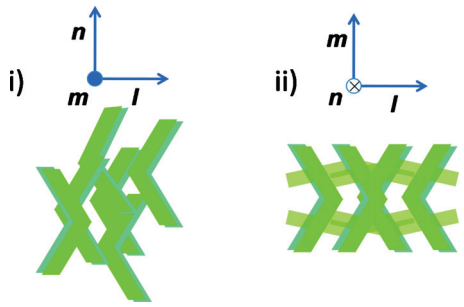

FIG. 1. Schematic of directors $\boldsymbol{n}$, $\boldsymbol{m}$, and $\boldsymbol{l}$ in bent core mesogens. Cases (i) and (ii) have been reported in different compounds (Refs. 4 and 6). [The lighter traces in (ii) indicate laterally attached aliphatic chains].

nematic phase behavior and stabilize the biaxial ordering by imposing steric constraints on the local reorientation of the molecular bent directions. The molecular packing in the nematic phases of these systems was determined by x-ray studies in both aligned and powder samples,[6,19] and it was found that under a magnetic field of appropriate strength, the molecules could align preferentially with the molecular bisector along the magnetic field direction and the molecular plane perpendicular to the director $\boldsymbol{n}$ [see Fig. 1 (ii)]. These findings are very important for the interpretation of the NMR results reported here.

In the search for the biaxial nematic phase, optical evidence has often been doubted owing to possible surface effects and x-ray evidence were distrusted because even if it shows the average correlation of mesogens along two directors, domains or aggregates may be still isotropically distributed about the direction of the **B** field. In an earlier study,[19] the influence of surface effects was reduced using a relatively thick oriented film and x-ray evidence was based on the results viewing perpendicular and parallel to the **B** field, thereby confirming two macroscopically oriented molecular axes in our partially deuterated sample. Techniques thought to determine without doubt the biaxial order of molecules in the bulk comprise of ^{2}H and ^{13}C solid state NMR.[4] The first can be performed either with selectively deuterated samples as in this study or with conveniently deuterated NMR probes.[3] The latter can be used on nonenriched samples. Indeed, it has been widely recognized that deuterium NMR measurements contribute decisively to the detection of biaxial nematic order. Specific experimental techniques, involving the combination of spectroscopy with sample's rotation or reorientations, have been developed in order to distinguish uniaxial from biaxial nematic phases. Reviews on NMR studies in N_B phases may be found in Refs. 3 and 20.

II. EXPERIMENTAL PROCEDURE

The synthesis of the selectively deuterated compound analyzed in this study (see Fig. 2) was described previously.[19,21] Note that the deuteron is placed in the para position at the end phenyl ring of one arm. ^{2}H NMR spectra were collected as a function of temperature using a BRUKER MSL 300 spectrometer with a magnetic field (**B**) strength of 7.049 T corresponding to a deuterium resonance frequency of 46.072 MHz. A quadrupolar echo sequence $[(\pi/2)_x$-τ-$(\pi/2)_y$-τ-echo] was used with a pulse spacing τ of

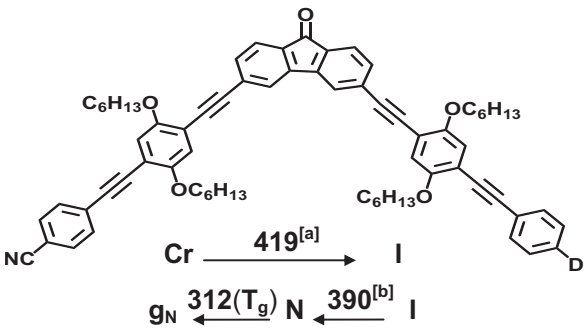

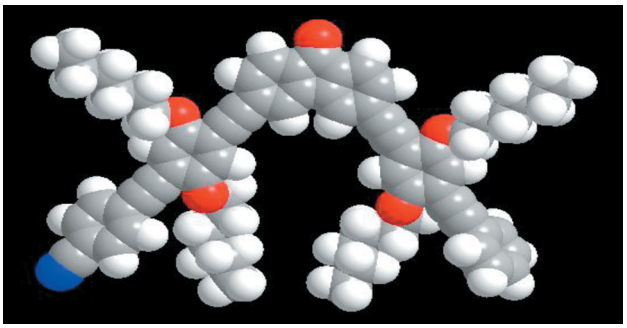

FIG. 2. Molecular structure and phase sequence of V-shaped mesogen. The transition temperatures are given in Kelvin ([a] POM data; [b] maximum of broad DSC peak).

20 μs, and a $\pi/2$ pulse length of 4.25 μs. ^{2}H NMR spectra were analyzed considering the possible presence of biaxial nematic ordering, which was previously detected in this system by other experimental methods including x-ray diffraction on aligned samples.[6,19] The NMR techniques usually used for the identification of the biaxial nematic ordering, namely, repeated 90° tilting or continuous rotation of the NMR sample around one axis perpendicular to the magnetic field was not applicable in this case. The limitation arose because of the progressive crystallization of this monotropic compound inside the **B** field, which severely weakened the NMR signal as the temperature was lowered and strongly shortened the effective time periods for data acquisition in the nematic phase, ruling out the long runs required by the above NMR techniques. Fortunately, the nematic director $\boldsymbol{n}$ orients normal to the static **B** field allowing us to probe the presence of biaxial ordering at low temperatures. This condition as well as the field-aligned $\boldsymbol{l}$ previously revealed by x-ray studies are confirmed by the simulations of ^{2}H NMR spectra reported in this work.

^{13}C NMR experiments were performed on a Varian Inova 400 spectrometer, using a Varian 3-channel 4 mm T-3 magic angle spinning (MAS) probe. The sample temperature was regulated by an air flow to better than 0.1 K. The two-dimensional (2D) rotor-synchronized pulse sequence [Fig. 3(a)] used here was introduced by Harbison *et al.*,[22] employing a single $\pi/2$ pulse of 4 μs width on the proton ^{1}H channel and detection on the ^{13}C channel after a cross polarization period of 2 ms, with a ^{1}H decoupling field of *ca.* 70 kHz. The MAS spinning rate $\omega_r/2\pi$ was set to 5000 Hz. 16 t_1 increments corresponding to a $\Delta t_1 = 12.5$ μs were used in the indirect dimension to cover one rotor period. Double Fourier transform with respect to the t_2 dimension as well as

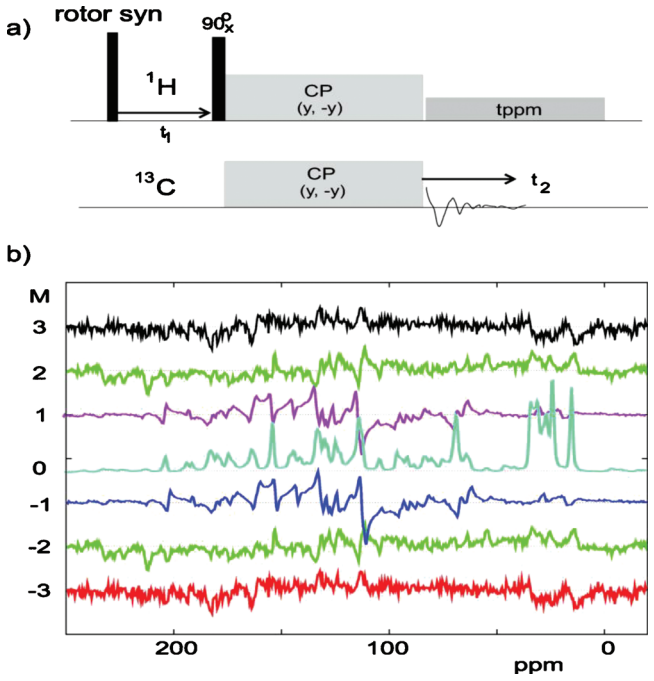

FIG. 3. (a) Rotor synchronized pulse sequence for 2D NMR. (b) Typical 2D ^{13}C MAS SS slices ($M=0$ is the central band) of an aligned biaxial glass in a MAS probe (without rotor spinning during the aligning process from the isotropic phase) at ambient temperature. Sample was spun at 5000 Hz in a **B** field of 9.4 T using pulse sequence (a). Signals above 160 ppm can be ascribed exclusively to SSs. Relative intensities of various M slices are scaled for clarity.

the rotor phase (in t_1) produced the observed 2D spectra. The observed f_1 slices correspond to different rotor phase angles (ϕ) that are incremented in the t_1 dimension according to $M\Delta\phi$ ($\Delta\phi=22.5°$) with $M=0, \pm 1, \ldots \pm 8$. $M=0$ gives a 1D spectrum which is collected at the start of the rotor period.

For the deuterium study, two different types of experiments were carried out due to the monotropic nature of the sample studied:

(A) In the first type, the sample was heated to a temperature slightly above the N-I transition (the isotropic phase is directly detected through the observation of a quadrupolar spectrum with a single narrow line, see Fig. 4, T_c+1 K) and then slowly cooled to the measuring temperature. The results of this set of experiments are presented in Fig. 4 (T_c+1 K: isotropic phase; T_c: I-N transition; T_c-1 K: uniaxial nematic phase; T_c-13 K: a wideline spectrum corresponding to a NMR signal with very poor signal-to-noise ratio probably associated to a biphase of nematic and crystalline domains).

(B) In the second set of experiments, the sample was heated to the isotropic phase then slowly cooled to T_c-2 K, stabilized for 10 min and then very rapidly cooled (in the presence of the **B** field) to a temperature (300 K) just below the glass transition and further below (250 K) in order to avoid the crystallization phenomenon that occurs when the sample is slowly cooled inside the **B** field.

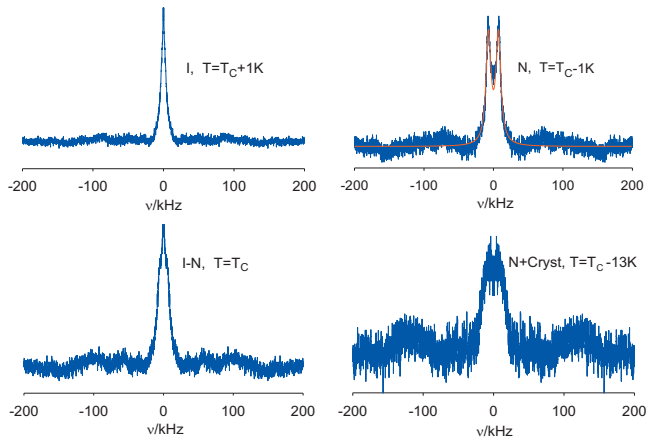

FIG. 4. Spectra collected as a function of temperature using the slow cooling procedure (from a temperature nearly above the I-N transition temperature T_c).

III. RESULTS AND DISCUSSION

The current shape-persistent BLC sample did not produce well-resolved ^{13}C NMR spectra in the nematic phase as the directors $\boldsymbol{n}$ are distributed perpendicular to the external **B** field.[6] However, a well resolved isotropic spectrum was easily obtained by means of MAS, a technique often employed in ^{13}C NMR of solids. In particular, we used a simple rotor-synchronized 2D ^{13}C experiment[22] to distinguish between phases with uniaxial and nonuniaxial phase symmetry.

For a sample with some sort of orientational order, as long as it does not possess a cylindrical symmetry about the rotor axis, the MAS sideband spectrum depends on the phase angle of the rotor at the start of the signal detection.[23] It is known that MAS spinning sideband (SS) observed in a single crystal can have absorptive or dispersive amplitudes, while from a crystalline power or any sample with a transverse isotropy SS shows always absorptive amplitudes.[24] Thus, the sample alignment inside the rotor is important to the success of getting meaningful sideband patterns. To prepare a proper nematic glass in the rotor, it was first heated to the isotropic phase in the MAS probe inside the **B** field and then rapidly cooled down to ambient temperature (298 K) under static condition so as to give a planar distribution of $\boldsymbol{n}$. This procedure is very important to guarantee that a nematic glass is obtained, otherwise the onset of crystallization is observed when the sample is slowly cool down inside the NMR **B** field. After a nematic glass has been prepared, the rotor was spun at 5000 Hz to do the 2D ^{13}C experiment using the pulse sequence in Fig. 3(a), and the 2D Fourier transform gives the M slices as shown in Fig. 3(b). It is recalled that M slices and $-M$ slices are symmetrical as observed in this work, while the sum of SS intensities $I_{M,N}$ (Ref. 23) for any slice parallel to f_2 axis is zero, except for the center slice ($M=0$), i.e.,

$$\Sigma I_{M,N}=0 \quad M\neq 0; \quad \Sigma I_{0,N}=1, \tag{1}$$

where N is the sideband number with the SS frequency in f_2 given as $N\omega_r/2\pi$, and the sum over N from $N=\infty$ to $N=-\infty$. The above symmetry properties for SS slices can be easily verified by inspection of Fig. 3(b). The biaxial glass was then heated to the high temperature nematic region to do the same 2D ^{13}C experiment at several temperatures. Figure

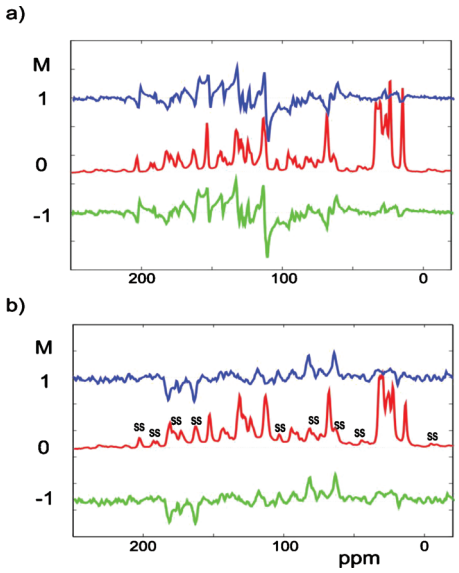

FIG. 5. ^{13}C MAS slices for $M=0$ and ± 1 for the biaxial glass at (a) 298 K and (b) uniaxial phase at 368 K. Only the $M=\pm 1$ slices are shown here which have been scaled up for clarity. SS denotes spinning sideband in the 1D spectrum.

5 shows some typical sideband spectra at two different temperatures, namely, 298 K (a) and 368 K (b). It is clear that for the nematic glass, the observed sidebands except the centerband ($M=0$) are dispersive with broad wings, which can be rationalized by the phase symmetry being nonuniaxial, while for the high temperature nematic at 368 K, sidebands for all M slices are absorptive. In the event that the nematic glass sample contains partially crystallized regions, the dispersive sidebands would each contain a small absorptive component from these regions. In fact, dispersive sidebands could not be identified at 298 K after the glass sample was left to fully crystallize outside the magnet for several weeks.[19] Figure 6 shows SS patterns at two different uniaxial nematic temperatures. Note that the absorptive SS can either be positive or negative, and Eq. (1) is still obeyed. Simple numerical simulation of SS of a typical ^{13}C site for a biaxial glass by integrating over the Euler angles (α,β) which transform between the rotor frame z axis and the molecule-fixed frame, did reveal dispersive sidebands as expected.[25]

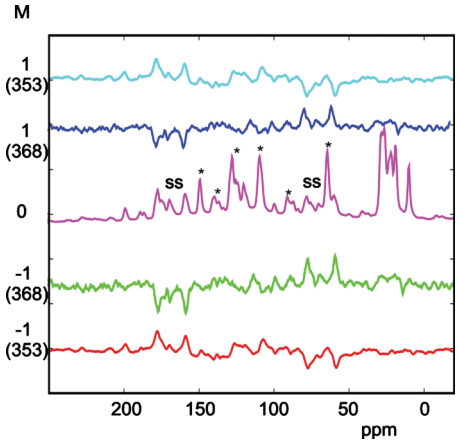

FIG. 6. ^{13}C MAS M slices at two different nematic temperatures. Number in parentheses denotes temperature in Kelvin, and * denotes ^{13}C peaks.

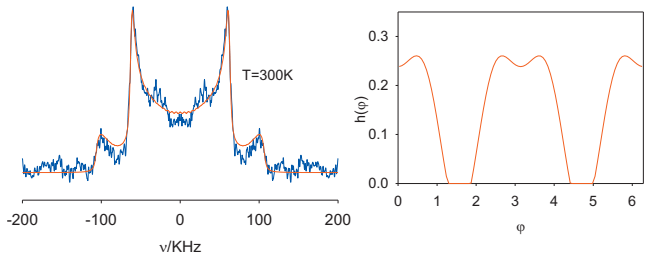

FIG. 7. (left) Spectra collected at $T=300$ K (blue line) and simulation (red line) using Eq. (4). (right) The φ dependence of the domain distribution function $h(\varphi)$ obtained from the fit and detailed later in the text.

^{2}H NMR spectra obtained in the type (B) way at 300 and 250 K are shown in Figs. 7 and 8, respectively. A 2D powderlike line shape is evident in these figures. More importantly the separation between the inner peaks in comparison with that of the outer shoulders reflects the presence of nonzero averaged asymmetry parameter η. In this study, the small intrinsic asymmetry (*ca.* 0.05) of the quadrupolar interaction for the aromatic deuteron is neglected.

A. Analysis of ^{2}H NMR data

The deuterium NMR spectrum arising from a single mesophase domain comprised of molecules with nonequivalent deuterated sites consists of pairs of lines, one for each site, centered at the Larmor precession frequency $(\nu_l = (1/2\pi)\gamma B)$ and separated by a frequency $\delta\nu_\iota$ (quadrupolar splitting) given by

$$\delta\nu_i = \frac{3}{2}\bar{\nu}_{Qi}\left(\frac{3}{2}\cos^2\beta_i - \frac{1}{2} + \frac{\eta_i}{2}\sin^2\beta_i\cos 2\alpha_i\right). \quad (2)$$

where $\bar{\nu}_{Qi}=(eQ/h)\bar{V}_{zz,i}$ is the averaged quadrupolar coupling constant, $\bar{V}_{\alpha\beta,i}$ is the motionally averaged electric field gradient tensor (EFG) at the nucleus site, e is the electron charge, Q is the quadrupolar moment of the deuterium nucleus, h is the Planck constant, $\eta_i=(\bar{V}_{xx,i}-\bar{V}_{yy,i})/\bar{V}_{zz,i}$ $(|\bar{V}_{xx,i}|\leq|\bar{V}_{yy,i}|\leq|\bar{V}_{zz,i}|)$ is the motionally averaged asymmetry parameter associated with site i, β_i and α_i are the polar and azimuthal angles that define the orientation of the static **B** field in the principal frame of the average EFG tensor $\bar{V}_{\alpha\beta,i}$ associated with each nonequivalent deuterated site (i) in the molecule. All other spin interactions beyond Zeeman and quadrupolar have been neglected. More conveniently the quadrupolar splitting in Eq. (2) can be expressed in a form

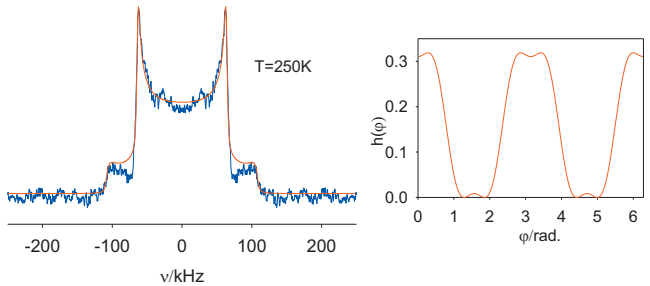

FIG. 8. (left) Spectra collected at $T=250$ K (blue line) and simulation (red line) using Eq. (4). (right) The φ dependence of the domain distribution function $h(\varphi)$ obtained from the fit and detailed later in the text.

that considers the different average EFG tensors of the various sites in a common reference frame fixed to the nematic domain, given as

$$\delta\nu_i = \frac{3}{2}\frac{eQ}{h}\left(\bar{V}_{zz,i}\left(\frac{3}{2}\cos^2\theta - \frac{1}{2}\right) + (\bar{V}_{xx,i} - \bar{V}_{yy,i})\frac{1}{2}\sin^2\theta\cos 2\varphi + \bar{V}_{xy,i}\sin^2\theta\sin 2\varphi + \bar{V}_{xz,i}\sin 2\theta\cos\varphi + \bar{V}_{yz,i}\sin 2\theta\sin\varphi\right), \quad (3)$$

where θ and φ are now the polar and azimuthal angles that define the orientation of the static NMR **B** field in the common reference frame and $\bar{V}_{\alpha\beta,i}$ the average EFG tensor components from the different sites in that frame that are related to their values in their principal frame through a coordinate transformation.

In a polydomain sample the distribution of domain orientations gives rise to a powder pattern that can be evaluated by adding up the contributions from the different domains weighted by the domain orientation distribution function, that is, the powder spectrum is given by the expression

$$G(\nu) = \int_0^{2\pi}\int_0^{\pi}\sum_{i=1}^{n}\{L(\nu - \delta\nu_i/2, \Delta\nu) + L(\nu + \delta\nu_i/2, \Delta\nu)\}P(\theta,\varphi)\sin\theta d\theta d\varphi, \quad (4)$$

where n is the number of nonequivalent sites in the molecules, $\delta\nu_i$ is given by Eq. (3), L is a Lorentzian shape function $(L(\nu,\Delta\nu) \equiv ((2\pi\Delta\nu)^{-1})/(1+(\nu/\Delta\nu)^2))$ of width $\Delta\nu$ at half height, $P(\theta,\varphi)$ represents the domain orientation distribution function relative to the **B** field, and θ and φ are defined above. In the final form of Eq. (4) the average EFG tensor components $\bar{V}_{\alpha\beta,i}$ were written in terms of $\bar{\nu}_{Qi} = (eQ/h)\bar{V}_{zz,i}$, $\eta_i = (\bar{V}_{xx,i} - \bar{V}_{yy,i})/\bar{V}_{zz,i}$, and the three Euler angles θ_i, φ_i, and ψ_i defining the orientation of the principal frame of $\bar{V}_{\alpha\beta,i}$ in the common frame. Next we discuss the determination of these parameters from the fittings of the experimental spectra to $G(\nu)$.

The high temperature spectrum reported in Fig. 4 just below the I-N transition is composed of two broad lines with a splitting of 15.8 kHz. From the x-ray studies[6] we know that the main director $\boldsymbol{n}$ is perpendicular to the field and on average to the molecular plane with a preferred orientation of the molecule's bisector along the field. A distribution of the bisector orientations relative to the field direction should produce a powder pattern unless the molecules rotate fast around the normal to the molecular plane. This fast rotation in the NMR time scale gives rise to a uniaxial average EFG tensor ($\eta_i = 0$), diagonal in the director frame with only one independent component $\bar{V}_{zz}$. In this case, Eq. (3) reduces to

$$\delta\nu = \frac{3}{2}\frac{eQ}{h}\bar{V}_{zz}\left(\frac{3}{2}\cos^2\theta - \frac{1}{2}\right) = \frac{3}{2}\bar{\nu}_Q\left(\frac{3}{2}\cos^2\theta - \frac{1}{2}\right) \quad (5)$$

with $\theta \approx \pi/2$. To generate the spectrum just below T_c using Eq. (4) with the splitting $\delta\nu$ given by Eq. (5), the distribution of domain orientations $P(\theta,\varphi)$ is approximated by

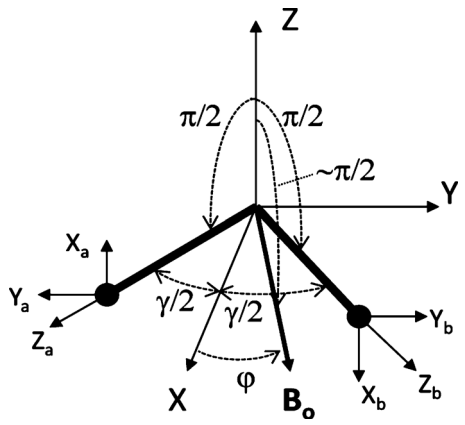

FIG. 9. Representation of the coordinate axis associated with the different frames considered in the powder pattern simulations at low temperatures. Sites a and b refer to equally populated orientations of V-shaped molecules in a domain. The round heads represent the deuterated positions and the thick line the molecular bodies.

$$P(\theta,\varphi) = \frac{1}{2\pi\sin(\theta)}g\left(\theta - \frac{\pi}{2}, \Delta\theta\right), \quad g(x,\Delta x) = ce^{-(x/\Delta x)^2}, \quad (6)$$

where the Gaussian $g(x,\Delta x)$ accounts for some static misalignment of the domain directors $\boldsymbol{n}$ with the normal to **B** and c is a normalizing constant. From the fit shown in Fig. 4, one obtains a value for $\bar{\nu}_Q = 21 \pm 3$ kHz and $\Delta\theta = 15 \pm 10°$ at $T = T_c - 1$ K.

The spectra collected at 300 and 250 K (see Figs. 7 and 8) are characteristic of powder patterns, thus implying a distribution of orientations of the principal axis of the average EFG tensors relative to the **B** field. This is compatible with the freezing of the fast molecular rotation around the molecular axis defining on average the main director. The partial alignment of the molecular bisector with the magnetic field observed by x-ray diffraction,[6,19] and in the present case obtained with the rapid cooling method, generates the orientation distribution responsible for the observed powder patterns.

A first inspection of the powder patterns shows the inner pair of sharp peaks having a frequency splitting larger than half the splitting between the outer shoulders. This reveals that the spectra are generated by 2D domain distributions and that these distributions are such that the **B** field is mainly distributed over the Y_aZ_a and Y_bZ_b planes of the principal frames of the averaged EFG tensors associated with sites a and b (see Fig. 9), remember that $(|\bar{V}_{xx,i}| \leq |\bar{V}_{yy,i}| \leq |\bar{V}_{zz,i}|)$. This is in complete agreement with the previous paragraph discussing the origin of the powder patterns. It is also seen that the outer shoulders are attenuated relative to cases with a uniform distribution of the **B** field over the Y_aZ_a and Y_bZ_b planes, and this effect indicates a nonuniform distribution and also a possible contribution from the finite duration of the rf pulses used. The effect of the finite duration of the rf pulses in the quadrupolar echo sequence on the powder spectra must be evaluated before carrying out the simulations. This is important in our case because the spectra are very wide and the $\pi/2$ rf pulses used were 4.25 μs long. This

TABLE I. Fitting parameters obtained from the spectra fits to Eq. (4) at low temperatures.

T (K)	$\bar{\nu}_Q$ (kHz)	η	γ (deg)	$\Delta\nu$ (kHz)	$\Delta\theta$ (deg)	c2	c4	c6
300	143 ± 6	0.17 ± 0.06	98 ± 5	3.9 ± 1.8	15	1.0 ± 1.5	-0.4 ± 0.9	0.0 ± 0.6
250	146 ± 6	0.18 ± 0.05	98 ± 5	3.2 ± 1.1	15	1.2 ± 0.9	0.0 ± 0.4	-0.2 ± 0.6

task was achieved by numerically integrating the Liouville/von Neumann[26] equation for a powder sample, considering the finite duration of the rf pulses. It was found that the spectra attenuation at higher frequencies is well accounted for through the multiplication of the spectra generated by Eq. (4) by a $(\sin(x)/x)^2$ function where $x=1.7\times10^{-5}\ \nu$ and ν is the frequency in hertz.

Taking these considerations into account, the simulation of the powder patterns is based on the scheme depicted in Fig. 9 indicating the different frames involved. According to the x-ray studies,[6,19] the molecular packing in the nematic phase depicted in Fig. 1 (ii) includes equal populations of molecules with orientations "a" and "b" as schematized in Fig. 9, where the round heads represent the deuterated position and the thick line the molecular bodies. Consequently, in each domain two nonequivalent sites are considered whose associated principal axis frames (for $\bar{V}_{\alpha\beta,i}$) are labeled, respectively, by a and b. The angle γ in between the two principal Z axis (Z_a,Z_b) of the average EFG tensors from the two sites may be larger or smaller than $\pi/2$ due to local molecular motions. The domain distribution function considered for the fits of the spectra at low temperatures is given by

$$P(\theta,\varphi)=\frac{1}{\sin(\theta)}g\left(\theta-\frac{\pi}{2},\Delta\theta\right)h(\varphi), \tag{7}$$

$$h(\varphi)=\frac{1}{2\pi}\max\left\{\begin{matrix}1+c2\cos(2\varphi)+c4\cos(4\varphi)+c6\cos(6\varphi)\\0\end{matrix}\right\},$$

based on the fact that the magnetic **B** field is approximately parallel to the molecular plane and that the bisector direction represented by the X axis is distributed according to $h(\varphi)$, expressed in terms of a truncated Fourier expansion with coefficients ci.

The spectra simulations generated by Eq. (4), with the domain orientation distribution given in Eq. (7), and corrected for the high frequency attenuation are shown as red lines in Figs. 7 and 8. The distribution function $h(\varphi)$ parameterized by the factors c2, c4, and c6 is used in each case. Note that $h(\varphi)$ peaks at $\varphi=0$ or π which is consistent with $\boldsymbol{l}$ being aligned preferentially along the magnetic field direction. The fitting parameters comprise $\bar{\nu}_Q$, η, γ, c2, c4, c6, $\Delta\theta$, and the Lorentzian linewidth $\Delta\nu$. The values obtained for these parameters are reported in Table I. Because $\Delta\theta$ is ill determined from each individual fit, we have chosen a common best value to all data fits.

These results allow us to draw significant conclusions: the finite η parameter obtained and the observation that the average EFG tensors from the two sites a and b do not share the same principal axis $(\gamma\neq90°)$ indicates that the mesophase domains do not exhibit D_{2h} symmetry but instead C_{2h} symmetry or lower. This may constitute a realization of the recent predictions[8] of biaxial nematic phases with symmetry lower than D_{2h}.

The averaged EFG tensor components $\bar{V}_{\alpha\beta,i}$ in the domain fixed (X',Y',Z') frame can be used to determine some or all the ordering matrix elements[27]

$$S_{lm}^{\alpha\beta}=\left\langle\frac{3}{2}\cos(\theta_{\alpha l})\cos(\theta_{\beta m})-\frac{1}{2}\delta_{\alpha\beta}\delta_{lm}\right\rangle.$$

The $\bar{V}_{\alpha\beta,i}$ are related to the EFG tensor components in a molecule fixed frame by the ordering matrix $S_{lm}^{\alpha\beta}$ according to

$$\bar{V}_{\alpha\beta,i}=\left(\frac{2}{3}S_{lm}^{\alpha\beta}+\frac{1}{3}\delta_{\alpha\beta}\delta_{lm}\right)V_{lm,i}. \tag{8}$$

Obtaining $\bar{V}_{\alpha\beta,i}$ values from the spectral fits and knowing $V_{lm,i}$ from solid state it is possible, in principle, to determine some or all the ordering matrix elements. The molecular and mesophase fixed frames must be defined before carrying out this calculation. According to the x-ray studies, we have considered that each mesophase domain is composed of molecules with orientations a and b whose orientational order is described by an ordering matrix. For convenience, the molecular (double primed) and domain (single primed) frames chosen are those indicated in Fig. 10.

The EFG tensors in the molecular (X'',Y'',Z'') frame for sites a and b are, respectively

$$[V]_a=\frac{h}{eQ}\nu_Q\begin{bmatrix}1&0&0\\0&-1/2&0\\0&0&-1/2\end{bmatrix},$$

$$[V]_b=\frac{h}{eQ}\nu_Q\begin{bmatrix}-1/2&0&0\\0&1&0\\0&0&-1/2\end{bmatrix}, \tag{9}$$

where $\nu_Q=185$ kHz is considered. Using these values in Eq. (8) we obtain

$$\bar{V}_{\alpha\beta,a} = \frac{h}{eQ}\nu_Q\left\{-\frac{1}{2}S^{\alpha\beta}_{Z''Z''} + \frac{1}{2}(S^{\alpha\beta}_{X''X''} - S^{\alpha\beta}_{Y''Y''})\right\},$$
$$\bar{V}_{\alpha\beta,b} = \frac{h}{eQ}\nu_Q\left\{-\frac{1}{2}S^{\alpha\beta}_{Z''Z''} - \frac{1}{2}(S^{\alpha\beta}_{X''X''} - S^{\alpha\beta}_{Y''Y''})\right\}. \quad (10)$$

Note that the same molecular frame (X'',Y'',Z'') was considered for a and b molecular orientations to write down the above equation. At $T=T_c-1$ K in the nematic phase the average EFG tensors from the two sites are equivalent and uniaxial, giving rise to only one independent term $\bar{V}_{Z'Z'}=(h/eQ)\bar{\nu}_Q$; using $\bar{\nu}_Q=21\pm3$ kHz in Eq. (10) we obtain $S^{Z'Z'}_{Z''Z''}=0.23\pm0.03$ and $S^{Z'Z'}_{X''X''}-S^{Z'Z'}_{Y''Y''}=0$. At low temperatures (300 and 250 K) the average EFG tensors from sites a and b are not equivalent and are given in the primed frame by (see Fig. 10 and Appendix A)

$$[\bar{V}]_a = \frac{h}{eQ}\frac{\bar{\nu}_Q}{4}\begin{bmatrix} 1-\eta+(\eta+3)\sin(\gamma) & (\eta+3)\cos(\gamma) & 0 \\ (\eta+3)\cos(\gamma) & 1-\eta-(\eta+3)\sin(\gamma) & 0 \\ 0 & 0 & 2(\eta-1) \end{bmatrix}, \quad (11a)$$

$$[\bar{V}]_b = \frac{h}{eQ}\frac{\bar{\nu}_Q}{4}\begin{bmatrix} 1-\eta-(\eta+3)\sin(\gamma) & (\eta+3)\cos(\gamma) & 0 \\ (\eta+3)\cos(\gamma) & 1-\eta+(\eta+3)\sin(\gamma) & 0 \\ 0 & 0 & 2(\eta-1) \end{bmatrix}. \quad (11b)$$

Using these values in Eq. (10) we obtain for the ordering matrix elements and their relevant combinations the following relations:

$$S^{Z'Z'}_{Z''Z''} = \left\langle \frac{3}{2}\cos^2\beta - \frac{1}{2}\right\rangle = \frac{\bar{\nu}_Q}{\nu_Q}(1-\eta),$$

$$S^{Z'Z'}_{X''X''} - S^{Z'Z'}_{Y''Y''} = \left\langle \frac{3}{2}\sin^2\beta\cos 2\delta\right\rangle = 0,$$

$$\frac{1}{3}[S^{X'X'}_{X''X''} - S^{X'X'}_{Y''Y''} - (S^{Y'Y'}_{X''X''} - S^{Y'Y'}_{Y''Y''})]$$
$$= \left\langle \frac{1+\cos^2\beta}{2}\cos 2\alpha\cos 2\delta - \cos\beta\sin 2\alpha\sin 2\delta\right\rangle$$
$$= \frac{\bar{\nu}_Q}{\nu_Q}\frac{(\eta+3)}{3}\sin\gamma, \quad (12a)$$

$$S^{X'X'}_{Z''Z''} - S^{Y'Y'}_{Z''Z''} = \left\langle \frac{3}{2}\sin^2\beta\cos 2\alpha\right\rangle = 0$$

$$S^{X'Y'}_{Z''Z''} = \left\langle \frac{3}{4}\sin^2\beta\sin 2\alpha\right\rangle = -\frac{\bar{\nu}_Q}{\nu_Q}\frac{\eta+3}{2}\cos(\gamma), \quad (12b)$$

$$S^{X'Y'}_{X''X''} - S^{X'Y'}_{Y''Y''} = \left\langle \frac{3}{2}\left[\frac{\cos^2\beta+1}{2}\sin 2\alpha\cos 2\delta + \cos\beta\cos 2\alpha\sin 2\delta\right]\right\rangle = 0, \quad (12c)$$

where we have included also the expressions of ordering matrix elements in terms of the Euler angles (α,β,δ) describing the orientation of the molecular frame in the phase frame. The ordering matrix elements and their relevant combinations' values for $T=300$ and 250 K are shown in Table II.

Using the expressions for the ordering matrix elements and their relevant combinations as functions of the Euler angles, it is possible to comment on the characteristics of the molecular motions capable of yielding the values encountered; $S^{Z'Z'}_{Z''Z''}$ is the nematic order parameter S and the value found (0.64–0.65) indicates that some degree of disorder is still present even at 250 K. The results $S^{X'X'}_{Z''Z''}-S^{Y'Y'}_{Z''Z''}=\langle(3/2)\sin^2\beta\cos 2\alpha\rangle=0$ and $S^{X'Y'}_{Z''Z''}=\langle(3/4)\sin^2\beta\sin 2\alpha\rangle=0.17$ can be accounted for if the molecular Z'' axis fluctuates in the phase frame with respect to Z' axis predominantly along the $\alpha=\pi/4, 5\pi/4$ directions; this motion corresponds probably to a molecular libration about an axis in the mo-

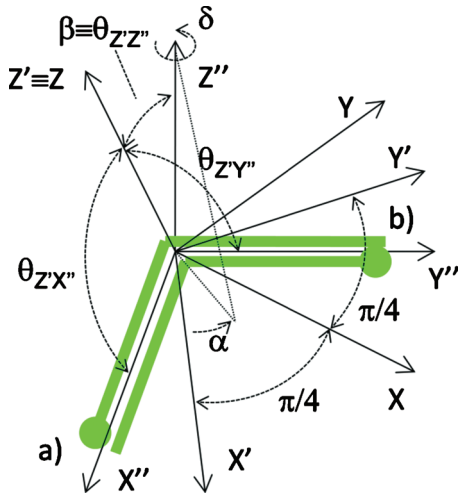

FIG. 10. Definition of the coordinate axis associated with the molecular (X'',Y'',Z'') and the phase domain (X',Y',Z') frames used in the determination of the ordering matrix elements. The coordinate axis (X,Y,Z) associated with the phase domain frame considered earlier is also shown.

TABLE II. Ordering matrix elements and their relevant combinations values determined from Eqs. (12a)–(12c).

Temperature (K)	$S_{Z''Z''}^{Z'Z'}$	$\frac{1}{3}[S_{X''X''}^{X'X'}-S_{Y''Y''}^{X'X'}-(S_{X''X''}^{Y'Y'}-S_{Y''Y''}^{Y'Y'})]$	$S_{Z''Z''}^{X'Y'}$
300	0.64 ± 0.05	0.81 ± 0.04	0.17 ± 0.10
250	0.65 ± 0.05	0.83 ± 0.04	0.17 ± 0.10

lecular plane perpendicular to the bisector. The fact that $(1/3)[S_{X''X''}^{X'X'}-S_{Y''Y''}^{X'X'}-(S_{X''X''}^{Y'Y'}-S_{Y''Y''}^{Y'Y'})]=\langle[(1+\cos^2\beta)/2]\cos 2\alpha\cos 2\delta-\cos\beta\sin 2\alpha\sin 2\delta\rangle$ is positive while $S_{X''X''}^{X'Y'}-S_{Y''Y''}^{X'Y'}=\langle(3/2)[[(\cos^2\beta+1)/2]\sin 2\alpha\cos 2\delta+\cos\beta\cos 2\alpha\sin 2\delta]\rangle=0$ is an indication of a strong correlation between the angles α and δ. When β is small the first expression can be approximated by $\langle([(1+\cos^2\beta)/4]+[(\cos\beta)/2])\cos(2\alpha+2\delta)\rangle$ and the second expression by $\langle(3/2)([(1+\cos^2\beta)/4]+[(\cos\beta)/2])\sin(2\alpha+2\delta)\rangle$, in the simplistic libration motion suggested above $\alpha=\pi/4\Rightarrow\delta=-\pi/4$ and $\alpha=5\pi/4\Rightarrow\delta=3\pi/4$ yielding $\sin(2\alpha+2\delta)=0$ and $\cos(2\alpha+2\delta)=1$. Finally the fact that $S_{X''X''}^{Z'Z'}-S_{Y''Y''}^{Z'Z'}=\langle(3/2)\sin^2\beta\cos 2\delta\rangle=0$ also fits the libration motion scenario since $\cos(2\delta)=0$ for $\delta=-\pi/4$ and $\delta=3\pi/4$.

IV. CONCLUSION

The observed ^{13}C NMR spectrum of an aligned sample is consistent with the ***n*** directors being distributed in a plane perpendicular to the **B** field in support of the x-ray results on this V-shaped mesogen. This is particularly useful to form the nematic glass inside the rotor before doing the rotor-synchronized 2D MAS NMR measurements. By means of SS patterns observed in the high temperature nematic phase and in the nematic glass, it is concluded that the latter does not possess uniaxial phase symmetry. This observation is corroborated by our ^{2}H NMR studies. The analysis of the DNMR spectra obtained at high temperature indicates that the molecules are rotating fast around the molecular plane normal, giving rise to a uniaxial nematic phase with a nematic order parameter of 0.23 found at T_c-1 K. At low temperature, just below the glass transition and well within the nematic glass, the 2D powder spectra obtained show a distribution $h(\varphi)$ of bisector orientations in the plane containing the external **B** field, which is peaked at the **B** direction. The two independent deuterated sites in each mesophase domain show a biaxial average EFG tensor and do not share the same principal axis indicating a lower than D_{2h} symmetry. The simulations are compatible with a C_{2h} symmetry (or lower) of the mesophase domains. The determined ordering matrix elements have allowed a simple characterization of the existing dominant molecular motion that is identified as librations with respect to an axis in the molecular plane perpendicular to the bisector.

Finally, the transition between the uniaxial nematic phase (observed at temperatures close to the N-I transition) and the biaxial nematic phase is probably associated to the freezing of the rotational movements around the molecular axis perpendicular to the molecular plane of the V-shaped mesogens.

ACKNOWLEDGMENTS

R.Y.D. wish to thank NSERC of Canada Grant No. RGPIN/3312 and M.L. the DFG LE 1571/2-1 for financial support. This work was partially supported by the Portuguese Science Foundation through project PTDC/FIS/65037/2006.

APPENDIX A: DERIVATION OF EQ. (11)

Equation (11) can be obtained starting from the average EFG tensors given for sites a and b in their respective principal frames a and b as indicated in the Fig. 9

$$[\bar{V}]_{a,\text{Paxis\_frame}}=\frac{h}{eQ}\bar{\nu}_Q\begin{bmatrix}\frac{\eta-1}{2} & 0 & 0\\ 0 & \frac{-\eta-1}{2} & 0\\ 0 & 0 & 1\end{bmatrix},$$
$$[\bar{V}]_{b,\text{Paxis\_frame}}=\frac{h}{eQ}\bar{\nu}_Q\begin{bmatrix}\frac{\eta-1}{2} & 0 & 0\\ 0 & \frac{-\eta-1}{2} & 0\\ 0 & 0 & 1\end{bmatrix}. \tag{A1}$$

Next these two tensors are evaluated in the primed frame (X',Y',Z') using the Wigner rotation matrices[28] according to the relations

$$V'_{ai}=\sum_{j=-2}^{j=2}V_{aj}D_{ij}^{2^*}(\pi/4-\gamma/2,\pi/2,\pi),$$
$$V'_{bi}=\sum_{j=-2}^{j=2}V_{bj}D_{ij}^{2^*}(\pi/4+\gamma/2,\pi/2,0), \tag{A2}$$

where V'_{ai} and V'_{bi} are the irreducible components of the average EFG tensors associated with sites a and b in the primed frame, $D_{ij}^{2^*}(\alpha,\beta,\delta)$ are the Wigner rotation matrix elements where the arguments α,β,δ are the Euler angles describing the orientations of frames a and b in the primed frame, and V_{aj} and V_{bj} are the irreducible components of the average EFG tensors associated with sites a and b in their principal frames (a) and (b). The transformation relations between the Cartesian and the irreducible components[28] are given by

$$V_0=\sqrt{\frac{3}{2}}V_{zz},\quad V_{\pm1}=\mp(V_{xz}\pm iV_{yz}),$$
$$V_{\pm2}=\frac{1}{2}(V_{xx}-V_{yy}\pm 2iV_{xy}). \tag{A3}$$

[1] M. J. Freiser, Phys. Rev. Lett. **24**, 1041 (1970).
[2] L. J. Yu and A. Saupe, Phys. Rev. Lett. **45**, 1000 (1980).
[3] G. R. Luckhurst, Thin Solid Films **393**, 40 (2001).
[4] L. A. Madsen, T. J. Dingemans, M. Nakata, and E. T. Samulski, Phys.

Rev. Lett. **92**, 145505 (2004); B. R. Acharya, A. Primak, and S. Kumar, *ibid.* **92**, 145506 (2004); R. Y. Dong, S. Kumar, V. Prasad, and J. Zhang, Chem. Phys. Lett. **448**, 54 (2007); V. Prasad, S.-W. Kang, L. Joshi, Q. Wang, and S. Kumar, J. Am. Chem. Soc. **127**, 17224 (2005).
[5] C. V. Yelamaggad, S. K. Prasad, G. G. Nair, I. S. Shashikala, D. S. S. Rao, C. V. Lobo, and S. Chandrasekhar, Angew. Chem., Int. Ed. **43**, 3429 (2004).
[6] M. Lehmann, S.-W. Kang, C. Köhn, S. Haseloh, U. Kolb, D. Schollmeyer, Q. Wang, and S. Kumar, J. Mater. Chem. **16**, 4326 (2006).
[7] C. D. Southern, P. D. Brimicombe, S. D. Siemianowski, S. Jaradat, N. Roberts, V. Görtz, J. W. Goodby, and H. F. Gleeson, EPL **82**, 56001 (2008); Y. Jang, V. P. Panov, A. Kocot, J. K. Vij, A. Lehmann, and C. Tschierske, Appl. Phys. Lett. **95**, 183304 (2009).
[8] H. R. Brand, P. E. Cladis, and H. Pleiner, Int. J. Eng. Sci. **38**, 1099 (2000); B. Mettout, Phys. Rev. E **74**, 041701 (2006); S. D. Peroukidis, P. K. Karahaliou, A. G. Vanakaras, and D. J. Photinos, Liq. Cryst. **36**, 727 (2009); P. K. Karahaliou, A. G. Vanakaras, and D. J. Photinos, J. Chem. Phys. **131**, 124516 (2009); M. V. Gorkunov, M. A. Osipov, A. Kocot, and J. K. Vij, Phys. Rev. E **81**, 061702 (2010).
[9] K. Severing and K. Saalwächter, Phys. Rev. Lett. **92**, 125501 (2004); K. Severing, E. Stibal-Fischer, A. Hasenhindl, H. Finkelmann, and K. Saalwachter, J. Phys. Chem. B **110**, 15680 (2006).
[10] K. Merkel, A. Kocot, J. K. Vij, R. Korlacki, G. H. Mehl, and T. Meyer, Phys. Rev. Lett. **93**, 237801 (2004); J. L. Figueirinhas, C. Cruz, D. Filip, G. Feio, A. C. Ribeiro, Y. Frère, T. Meyer, and G. H. Mehl, *ibid.* **94**, 107802 (2005); K. Neupane, S. W. Kang, S. Sharma, D. Carney, T. Meyer, G. H. Mehl, D. W. Allender, S. Kumar, and S. Sprunt, *ibid.* **97**, 207802 (2006); C. Cruz, J. L. Figueirinhas, D. Filip, G. Feio, A. C. Ribeiro, Y. Frère, T. Meyer, and G. H. Mehl, Phys. Rev. E **78**, 051702 (2008).
[11] P. H. J. Kouwer and G. H. Mehl, J. Am. Chem. Soc. **125**, 11172 (2003).
[12] E. Date and D. W. Bruce, J. Am. Chem. Soc. **125**, 9012 (2003).
[13] A. Stroobants and H. N. W. Lekkerkerker, J. Phys. Chem. **88**, 3669 (1984).
[14] A. G. Vanakaras and D. J. Photinos, Mol. Cryst. Liq. Cryst. **299**, 65 (1997); A. G. Vanakaras, S. C. McGrother, G. Jackson, and D. J. Photinos, *ibid.* **323**, 199 (1998); A. G. Vanakaras, A. F. Terzis, and D. J. Photinos, *ibid.* **362**, 67 (2001).
[15] P. Palffy-Muhoray, J. R. De Bruyn, and D. A. Dunmur, J. Chem. Phys. **82**, 5294 (1985).
[16] D. W. Bruce, Chem. Rec. **4**, 10 (2004).
[17] R. Berardi, L. Muccioli, S. Orlandi, M. Ricci, and C. Zannoni, J. Phys.: Condens. Matter **20**, 463101 (2008).
[18] D. Apreutesei and G. H. Mehl, Chem. Commun. (Cambridge) **2006**, 609.
[19] M. Lehmann, C. Köhn, J. L. Figueirinhas, G. Feio, C. Cruz, and R. Y. Dong, Chem.-Eur. J. **16**, 8275 (2010).
[20] K. Severing and K. Saalwächter, *Thermotropic Liquid Crystals, Recent Advances* (Springer, Netherlands, 2007).
[21] M. Lehmann, Ch. Köhn, H. Kresse, and Z. Vakhovskaya, Chem. Commun. (Cambridge) **2008**, 1768.
[22] G. S. Harbison, V.-D. Vogt, and H. W. Spiess, J. Chem. Phys. **86**, 1206 (1987).
[23] K. Schmidt-Rohr and H. W. Spiess, *Multidimensional Solid-State NMR and Polymers* (Academic, London, 1994), p. 372.
[24] M. M. Maricq and J. S. Waugh, J. Chem. Phys. **70**, 3300 (1979).
[25] M. Veshtort and R. G. Griffin, J. Magn. Reson. **178**, 248 (2006).
[26] R. Kimmich, *NMR: Tomography, Diffusometry, Relaxometry* (Springer-Verlag, Berlin, 1997).
[27] J. Prost and P. G. de Gennes, *The Physics of Liquid Crystals* (Clarendon, Oxford, 1996).
[28] D. A. Varshalovich, A. N. Moskalev, and V. K. Khersonskii, *Quantum Theory of Angular Momentum* (World Scientific, Singapore, 1988).